Supporting Information

Doping induced band-gap shrinkage to modify electronic structure of MoS_2 for organic wastewater management

Yuchen Zhang [a, b, c], Yuehan Jia [a, b, c], Yanjie Li [a, b, c], Hongquan Xu [a, b, c], Jingsu Wang [a, b, c], Maobin Wei [a, b, c], Yong Zhang [a, b, c*], Hui Yuan [d*], Ming Gao [a, b, c*]

a. Key Laboratory of Functional Materials Physics and Chemistry of the Ministry of Education, Jilin Normal University, Changchun, 130103, P. R. China

b. National Demonstration Centre for Experimental Physics Education, Jilin Normal University, Siping, 136000, P. R. China

c. Key Laboratory of Preparation and Application of Environmental Friendly Materials, Jilin Normal University, Ministry of Education, Changchun, 130103, P. R. China

d. State Key Laboratory of Catalytic Materials and Reaction Engineering, SINOPEC Research Institute of Petroleum Processing Co. Ltd., Beijing, 100083, China

*Corresponding author: Yong Zhang, Hui Yuan, Ming Gao

*Corresponding author at: Key Laboratory of Functional Materials Physics and Chemistry of the Ministry of Education, and National Demonstration Centre for Experimental Physics Education, Jilin Normal University, Siping 136000, People's Republic of China.

Tel.: +86 434 3294566;

fax: +86 434 3294566;

Email address: zhangyong@jlnu.edu.cn (Y. Zhang); yuanhui.ripp@sinopec.com (H. Yuan); gaomingphy@126.com (M. Gao)

1. Experimental section

1.1 Materials

Ammonium molybdate ($[(NH_4)_6Mo_7O_4 \cdot 2H_2O]$, ≥99.5%), thiourea ($NH_2CSNH_2$, ≥99%), ruthenium (III) chloride hydrate ($RuCl_3 \bullet xH_2O$, ≥99%), crystal violet (CV), congo Red (CR) and rhodamine 6G (R6G) were purchased from Sigma Aldrich. There was no further purification of any of the chemicals.

1.2 Preparation of MoS_2 and Ru-MoS_2

MoS_2 and Ru-MoS_2 One-step hydrothermal method was used to synthesis MoS_2 and MoS_2-based nanoflowers. Firstly, 1.2358 g $[(NH_4)_6Mo_7O_4 \cdot 2H_2O]$ and 2.5120 g of NH_2CSNH_2 were dissolved in 60 mL of deionized water. The mixture was stirred with a magnetic stirrer for 30 minutes. Then $RuCl_3 \cdot xH_2O$ were added into the above solution. The mixture was continuously stirred until completely dissolved. Secondly, the above mixed solution was transferred into a 100 ml Teflon-lined stainless steel autoclave and heated at 220 °C for 18 h. After cooling down to room temperature, the collected black precipitate was washed three times with deionized water and alcohol, respectively. Finally, the sediment in 60 ℃ drying oven dry after 6 h to get the black solid powder. For comparison, MoS_2 was also synthesized via adopting the same approach without addition of $RuCl_3 \cdot xH_2O$.

1.3 Characterization

The structural and geometrical analysis of the prepared samples along with X-ray

powder diffraction (XRD). The diffraction patterns were collected on a Rigaku D/Max 3C XRD using Cu Kα radiation (λ = 1.542 Å) with a step size 0.02° in the range (2θ) from 5° to 80°. The surface morphology, microstructural analysis, and elemental analysis of the fabricated samples were described using scanning electron microscopy (SEM, JSM-7800F) and a transmission electron microscope (TEM, JEM-2100HR). Besides, to determine the surface chemical composition, X-ray photoelectron spectroscopy (XPS, Thermo ESCALAB 250) measurements were carried out. The SERS spectra were detected under a 514.5 nm (2.41 eV) Ar^+ ion laser, the Renishaw inVia Raman system. Ultraviolet (UV)-vis absorption spectra were measured with a Hitachi U-3600 spectrophotometer (Shimadzu, Japan).

1.4 Detection of CV, CR and R6G by all substrates

Firstly, 10^{-3} M CV, CR and R6G were selected as the SERS model probes to verify the optimal SERS activity of all substrates. In order to ensure adequate contact between substrates and molecules, all samples were mixed with CV solution and shook for 2 h. Then, Ru-MoS_2 substrate was mixed with CV solution to test for stability, recyclability and uniformity. In these SERS tests, the 514.5 nm laser power is 10 mW, attenuation 100%, exposure time is 20 s, and 3 accumulations every spectrum.

1.5 Photocatalysis experiment

The photocatalytic activities of different synthesized samples were estimated by degrading four dyes under a 300 W xenon arc lamp with a 420 nm cut-off filter to ensure the desired irradiation light. Specifically, 10 mg of the prepared samples and 25

mL of 10^{-3} M R6G, CV and CR were mixed under magnetic stirring in the dark at ambient temperature for 30 min to establish adsorption-desorption equilibrium. When the photocatalytic reaction was running, 1 mL of the resultant dispersion solution subjected to light irradiation was collected and the photocatalysts were removed by centrifugation at different intervals. The residual concentration of R6G, CV and CR in the reaction mixture was monitored by a UV-vis spectrometer. The degradation of dyes was fitted and studied by the pseudo first-order reaction namely, Langmuir-Hinshelwood model $\ln(c_t/c_0)= -kt$, where k is the reaction rate constant per minute, whereas t is time of reaction in minute, and C_t and C_0 are the reaction concentrations at final and initial time, respectively.

1.6 Radical scavenger tests

Free radical scavenging experiments were designed to determine the contribution of different reactive species and investigate the photoreaction mechanism over Ru-MoS_2 composite. Specifically, silver nitrate ($AgNO_3$, 1.0 mM), ethylenediaminetetracetic acid (EDTA, 10% v/v), and isopropanol (IPA, 10% v/v) were applied to scavenge the superoxide radical ($\bullet O^-_2$), holes (h^+) and hydroxyl radicals ($^\bullet OH$), respectively.

1.7 Computational details

The density functional theory method was used to implement the entire calculation in the Dmol 3 program. To handle electron exchange and correlation, the Perdew-

Burke-Ernzerhof (PBE) function with generalized gradient approximation (GGA) was used. To address the relativistic effect of the Ru atom, we selected the DFT semicore pseudopotential (DSSP) approach and double numerical plus polarization (DNP) as the atomic orbital basis set. The Tkatchenko and Scheffler (TS) approach was used to gain a deeper comprehension of the van der Waals interaction. For geometric optimization and electronic structure computations, the Monkhorst−Pack k-point mesh of 10 × 10 × 1 was taken for the Brillouin zone integration. We decided on 10^{-4} Ha for the energy tolerance accuracy, 2 × 10^{-2} Ha/Å for the maximum force, and 5 × 10^{-2} Å for the displacement. To provide correct findings for total energy estimates in static electronic structure calculations, a 10^{-6} Ha self-consistent loop energy, a global orbital cutoff radius of 5.0 Å, and a smearing of 0.005 Ha were used. Each and every calculation was spinpolarized.

2. Results and discussion

Table S1 Raman peak assignments for CV.

Crystal Violet (cm^{-1})	Raman Vibrational band assignments
805	Phenyl-H out-of-plane antisymmetric bending
914	Phenyl ring breathing mode
1178	C-phenyl, C–H in-plane antisymmetric stretching
1373	C–N, Phenyl-C-phenyl antisymmetric stretching
1587	C-phenyl in-plane antisymmetric stretching
1621	C-phenyl in-plane antisymmetric stretching

Table S2 Comparison of enhancement factor of CV on all substrates.

CV	MoS_2	Ru-MoS_2	MoS_2@Cu_2S
EF	1.21×10^4	3.61×10^8	2.99×10^8

Table S3 Raman peak assignments for CR

Congo Red	Raman Vibrational band assignments
481	rocking vibrations in the benzene ring
1006	the ring breathing
1270	N-phenyl stretch in the benzene ring
1390	-OH and -SO_3Na in-plane bending
1432	C-C stretching in the benzene ring
1490	
1565	the ring stretching
1606	C=C stretching in the benzene ring

Table S4 Raman peak assignments for R6G

Rhodamine 6G	Raman Vibrational band assignments
612	In plane C–C–C bending
772	Out of plane C–H bending
1188	In plane Xanthenes ring deformation, C–H bending, N–H bending
1364	Xanthenes ring stretching, in plane C–H bending
1649	Xanthenes ring stretching, in plane C–H bending

Table S5 The enhancement factor and detection limit on the Ru-MoS_2 substrate

compared with other semiconductors materials.

SERS substrates	LOD(mol L^{-1}))	EF	References
$MoS_2/TiO_2/Au$	10^{-9}	1.57×10^5	Q. Wei, Q. Dong, et al. Spectrochim. Acta A, 285 (2023) 121895.
F_4TCNQ/MoS_2	10^{-10}	2.53×10^6	M. Liu, W. Liu,et al. ACS Appl. Mater. Interfaces, 14 (2022) 56975-56985.
MoS_2/ZnS	10^{-12}	1.13×10^6	Y. Quan, J. Yao, et al. Sensors Actuat. B-Chem. 327 (2021) 128903.
$CC/MoS_2/Ag/PDMS$	10^{-12}	10^7	D. Wu, J. Chen, et al. J. Mater. Chem. C, 6 (2018) 12547-12554.
$Ag\text{-}MoS_2$	10^{-9}	10^7	J. Singh, R. Soni, et al. Chemosphere, 339 (2023) 139735.
$Ru\text{-}MoS_2$	**10^{-11}**	**3.61×10^8**	**This work**

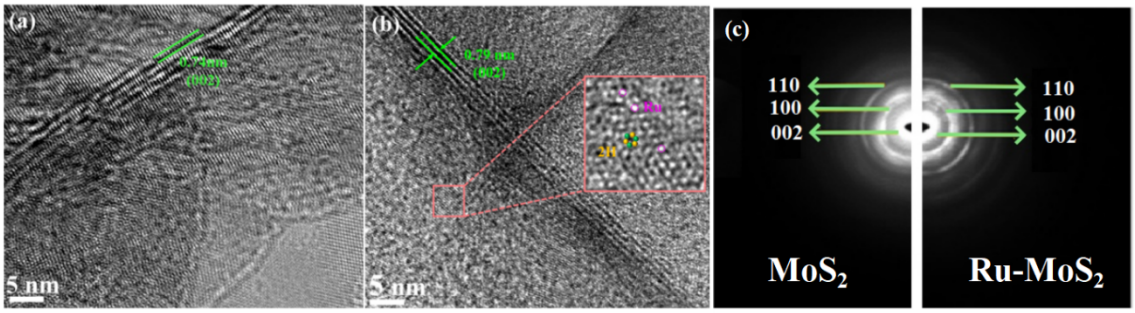

Figure S1 HRTEM images of (a) MoS_2 and (b) $Ru\text{-}MoS_2$. (c) SAED pattern of MoS_2 and $Ru\text{-}MoS_2$.

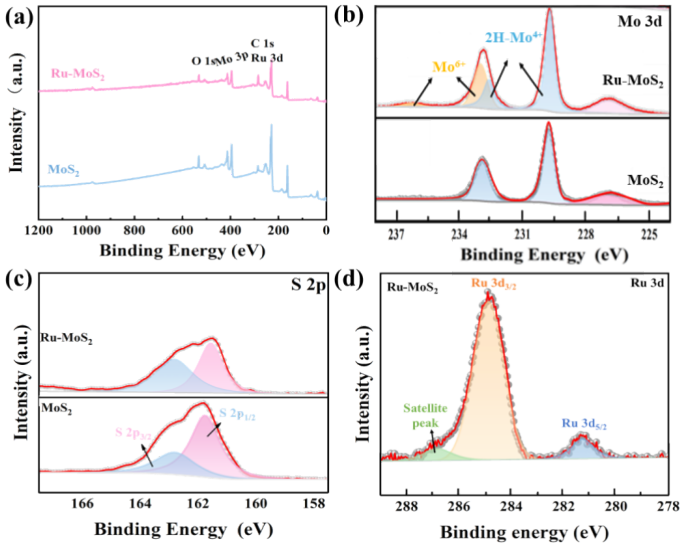

Figure S2 (a) XPS survey spectrum of MoS_2 and Ru-MoS_2, XPS spectra of (b) Mo 3d, (c) S 2p core level for MoS_2 and Ru-MoS_2; (d) Ru 3d core level for Ru-MoS_2.

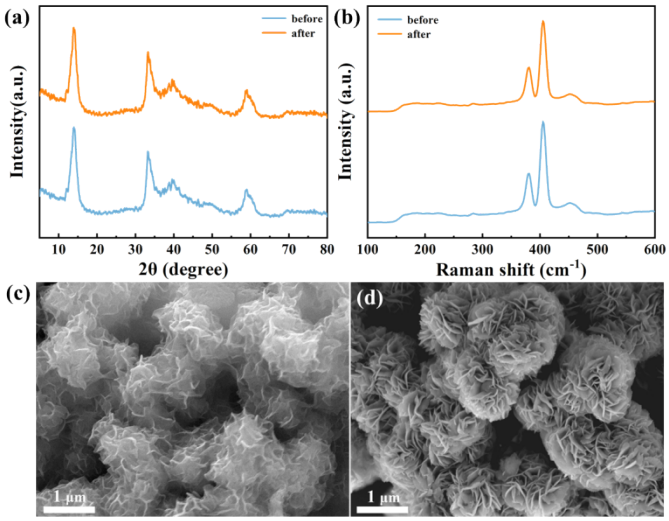

Figure S3 (a) XRD, (b) Raman, (c) and (d) SEM images of Ru-MoS_2 before and after 5 cycle.

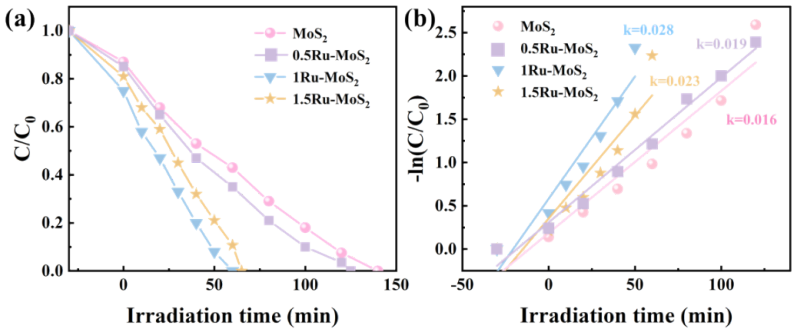

Figure S4 UV-vis spectra during UV-Vis light irradiation of (a) 10^{-3} M CV and kinetic modeling studies of (b) CV.

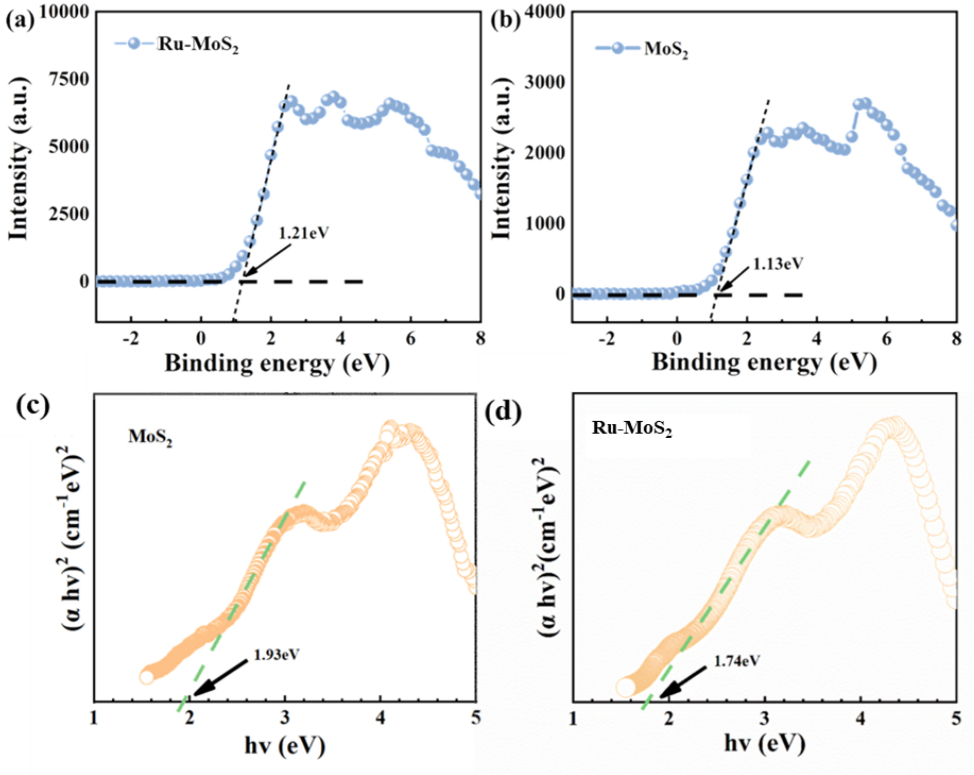

Figure S5 Determinations of VB using XPS of (a) Ru-MoS_2 and (b) MoS_2; (c) optical energy band gap of MoS_2 and (d) optical energy band gap of Ru-MoS_2 .

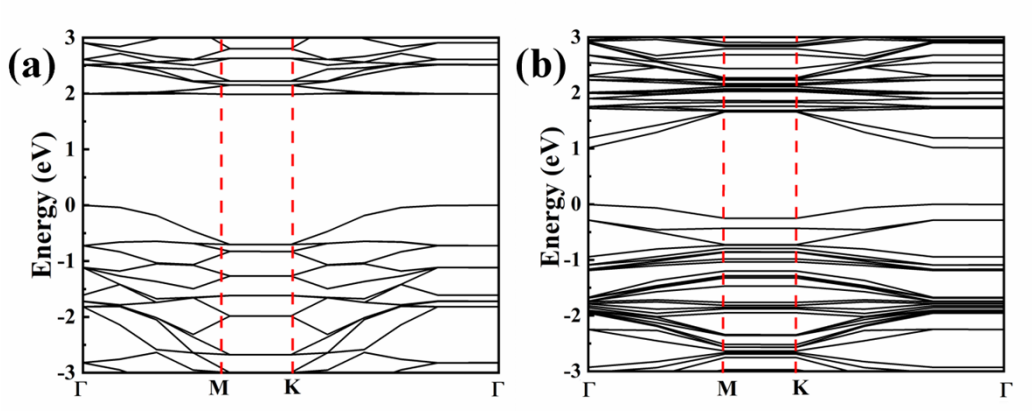

Figure S6 Band structure of MoS_2 and Ru-MoS_2.

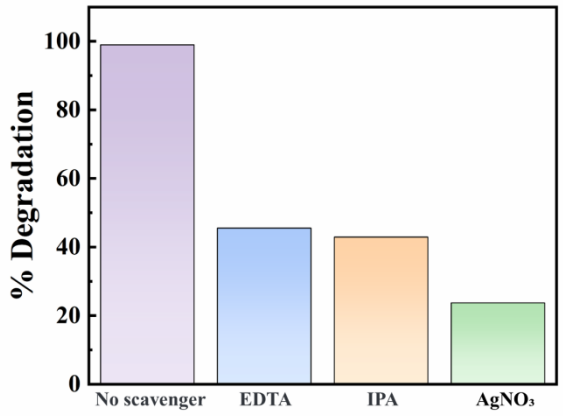

Figure S7 Effect of different scavengers on photocatalytic degradation of CV.

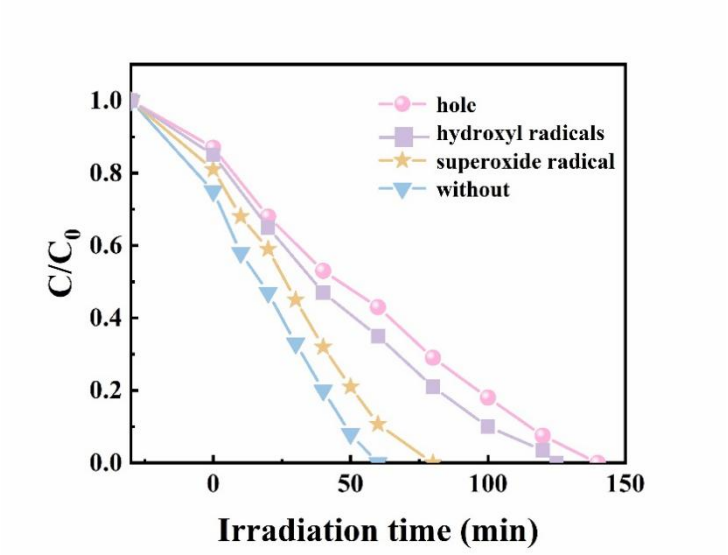

Figure S8 Influence of scavengers on photocatalytic performance of Ru-MoS_2.

Note 1.

The enhancement factor (EF) is calculated according to the following equation:

$$EF = \frac{I_{SERS}}{I_{NRF}} \times \frac{N_{NRF}}{N_{SERS}}$$

Where N_{SERS} and N_{REF} are the number of probe molecules in the excitation volume of the CV/Ru-MoS_2 substrate and reference, respectively. I_{SERS} and I_{REF} are respectively the Raman signal intensities at 1626 cm^{-1} obtained from 10^{-3} M CV molecules on the CV/Ru-MoS_2 substrate and 10^{-3} M CV molecules on bare glassware, while sample was excited under 514 nm laser irradiation.For the calculation of N_{SERS}, 0.1 μl (V_1) from 10^{-4} M (C_1) CV solution was adsorbed on the surface of the 16 mm^2 (S_1). The Raman's laser spot diameter was about 5 μm (d). The number of excited probe molecules were calculated in the following way:

$$N_{SERS} = (\frac{\pi d^2}{4 \times S_1}) \times V_1 \times C_1 \times N_A$$

For the calculation of N_{REF}, the laser was passed through the CV solution ($C_2 = 10^{-3}$ M), and the illuminated volume (V_2) was about 6.25×10^{-14} m^3. The number of probe molecules being illuminated in the reference Raman measurement was calculated as:

$$N_{REF} = V_2 \times C_2 \times N_A$$

From this, the EF of different samples can be calculated separately.

Note 2.

The Fermi level (E_F) can be determined using the relationship with the flat-band potential (V_{fb}):

$$E_F = -eV_{fb}$$

Where e is the elementary charge. The potential conversion relationship between standard hydrogen electrode (SHE) and Ag/AgCl reference electrode (3.5 M KCl solution) is $E_{SHE} = E_{Ag/AgCl} + 0.205$ V. The absolute potential value for SHE is taken as -4.5 V. Therefore, the Fermi level in reference to vacuum can be calculated as:

$$E_{F,vacuum} = e[-4.5-(V_{fb,Ag/AgCl}+0.205)]eV$$

Combining with XPS valence band spectra, the discrepancy between E_f and VB can be determined, while using diffuse reflectance spectra the band gap between VB and CB can be determined.